Matched-filter coding of sky polarization results in an internal sun compass in the brain of the desert locust

Frederick Zittrell[a,b], Keram Pfeiffer[c,1], and Uwe Homberg[a,b,1,2]

[a]Department of Animal Physiology, Philipps-University Marburg, 35032 Marburg, Germany; [b]Center for Mind, Brain and Behavior (CMBB), Philipps-University Marburg and Justus Liebig University Giessen, 35032 Marburg, Germany; and [c]Biocenter, Behavioral Physiology and Sociobiology, University of Würzburg, 97074 Würzburg, Germany

Edited by John G. Hildebrand, University of Arizona, Tucson, AZ, and approved August 3, 2020 (received for review March 19, 2020)

Many animals use celestial cues for spatial orientation. These include the sun and, in insects, the polarization pattern of the sky, which depends on the position of the sun. The central complex in the insect brain plays a key role in spatial orientation. In desert locusts, the angle of polarized light in the zenith above the animal and the direction of a simulated sun are represented in a compass-like fashion in the central complex, but how both compasses fit together for a unified representation of external space remained unclear. To address this question, we analyzed the sensitivity of intracellularly recorded central-complex neurons to the angle of polarized light presented from up to 33 positions in the animal's dorsal visual field and injected Neurobiotin tracer for cell identification. Neurons were polarization sensitive in large parts of the virtual sky that in some cells extended to the horizon in all directions. Neurons, moreover, were tuned to spatial patterns of polarization angles that matched the sky polarization pattern of particular sun positions. The horizontal components of these calculated solar positions were topographically encoded in the protocerebral bridge of the central complex covering 360° of space. This whole-sky polarization compass does not support the earlier reported polarization compass based on stimulation from a small spot above the animal but coincides well with the previously demonstrated direct sun compass based on unpolarized light stimulation. Therefore, direct sunlight and whole-sky polarization complement each other for robust head direction coding in the locust central complex.

sky compass | polarized light | spatial orientation | central complex | desert locust

Animals need to navigate effectively through their environment, be it for foraging, mating, or migration. One aspect of spatial navigation is a sense of direction. In mammals, certain neurons of the hippocampal formation and associated areas fire maximally when the animal's head faces a particular direction (1–3). These neurons are termed "head direction cells." They encode head orientation based on visual background information, memory, and self-motion cues (3). A simple version of a head direction network has also been found in insects. Here neurons of the central complex (CX) encode heading direction to control turns in flight or walking (4–8). In the fruit fly *Drosophila*, Ca^{2+} imaging revealed a bump of activity that shifts through the columns of the ellipsoid body, fan-shaped body, and protocerebral bridge (PB), three substructures of the CX, as the fly turns, mapping the 360° space around the fly in a compass-like manner (4, 7, 8). Manipulating the position of the bump experimentally leads to shifts in flight orientation relative to the bump, indicating that the activity bump not only monitors head directions but actually controls them (9, 10). Whereas in the fly visual landscape information seems to play a major role in generating and updating the internal representation of heading in the CX (4, 5, 10), work in the desert locust, monarch butterfly, dung beetle, and bee showed that neurons are highly sensitive to celestial cues, including the sun and the sky polarization pattern (11–14). Nevertheless, flies, too, perform menotactic orientation with respect to sky polarization or a simulated sun (15, 16). Sun compass orientation is lost after silencing a particular CX cell type, suggesting that the CX in *Drosophila*, like in other insects, is also involved in celestial navigation. The polarization pattern of the sky is generated by the sun: sunlight is scattered at air molecules in the atmosphere and becomes partly linearly polarized in a systematic manner, which produces a polarization pattern in the sky (Fig. 1*A*). This pattern directly depends on the position of the sun, thereby signaling the solar azimuth, making it suitable for celestial navigation.

Field observations showed that several insect species including desert ants (17), honey bees (18), monarch butterflies (19), and dung beetles (20) use the polarization pattern of the sky for spatial orientation while in others [field crickets (21), desert locusts (22), and fruit flies (23, 24)], laboratory studies demonstrated orientation depending on the angle of polarization (AoP) of dorsally presented light. The AoP of light is detected by photoreceptors in specialized dorsal rim areas of the compound eyes (25). From the dorsal rim areas of both eyes, polarization vision pathways converge via the optic lobes, anterior optic tubercles, and lateral accessory lobes on the lower division of the central body (CBL), equivalent to the ellipsoid body in flies. Signals are processed further in the PB and upper division of the CBL (equivalent to fan-shaped body in flies) and are believed to affect descending pathways for motor control in the paired lateral accessory lobes adjacent to the CX (26) (Fig. 1 *B* and *C*). The CX is organized in layers and columns, which are mainly interconnected by neurons of two categories: tangential neurons

Significance

Many animals rely on the sun as a reference during spatial orientation. Insects can also use the pattern of polarization of the sky, generated by scattering of sunlight, as a guiding cue. We show here that certain neurons in the protocerebral bridge of the brain of the desert locust encode particular sun positions by responding best to a pattern of polarization generated by those sun positions. Across the protocerebral bridge, these neurons are arranged in a topographic, 360° compass with respect to angular orientation to the sun. This polarization-based compass is in line with a previously reported compass based on direct sunlight. Therefore, direct sunlight and whole-sky polarization complement each other in head direction coding in the locust.

Author contributions: F.Z., K.P., and U.H. designed research; F.Z. performed research; K.P. contributed analytic tools; F.Z. analyzed data; and F.Z., K.P., and U.H. wrote the paper.

The authors declare no competing interest.

This article is a PNAS Direct Submission.

[1]K.P. and U.H. contributed equally to this work.

[2]To whom correspondence may be addressed. Email: homberg@staff.uni-marburg.de.

This article contains supporting information online at https://www.pnas.org/lookup/suppl/doi:10.1073/pnas.2005192117/-/DCSupplemental.

First published September 28, 2020.

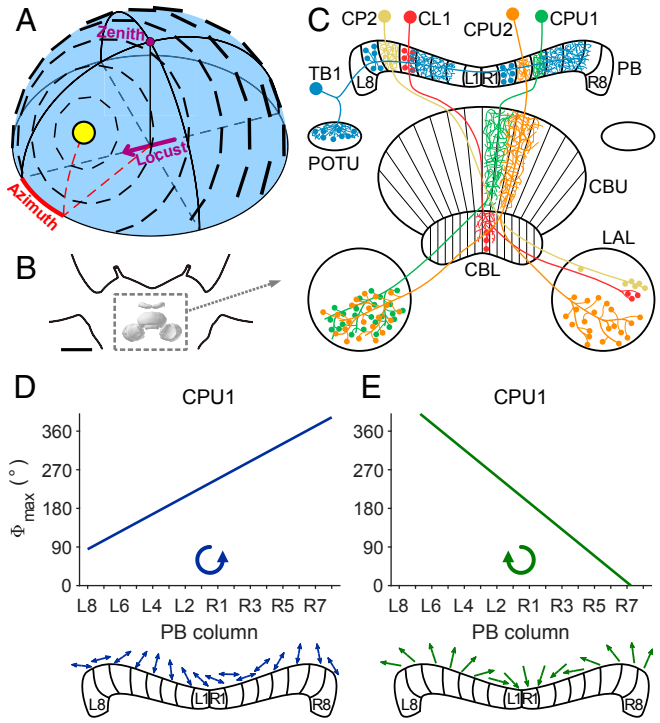

Fig. 1. Celestial compass cues and compass coding in the CX. (*A*) Schematized polarization pattern of the sky as produced by the sun at 40° elevation and 30° azimuth relative to an observer indicated by the purple arrow. Bar orientation and thickness indicate AoP and degree of polarization, respectively. (*B*) Frontal diagram of the locust brain indicating the location of the CX (boxed in dashed lines). Reprinted by permission from ref. 63, Springer Nature: Cell and Tissue Research, copyright (2008). (*C*) Schematic drawing of the locust CX with cell types investigated in this study. Fine branches indicate smooth (dendritic) arborizations, small dots symbolize varicose (presynaptic) arborizations, and large dots represent somata. Columnar neurons (CL1, CP2, CPU1, and CPU2) exist as isomorphic sets of 16 neurons, covering all 16 columns of the PB. Tangential neurons (TB1) exist as four subtypes per brain hemisphere, each having varicose ramifications in two columns that are eight columns apart. (*D* and *E*) Topographic representation of AoP to zenithal stimulation with blue polarized light (*D*) and azimuth of a green LED (*E*) in the same set of CPU1 neurons innervating different columns of the PB. The tuning to AoP changes from L8 to R8 in counterclockwise manner (*D, Bottom*), and the azimuth tuning changes in clockwise fashion (*E, Bottom*). CBL, lower division of the central body; CBU, upper division of the central body; L1 and L8, innermost, respectively outermost column in the left hemisphere of the PB; LAL, lateral accessory lobe; POTU, posterior optic tubercle; R1 and R8, innermost, respectively outermost column in the right hemisphere of the PB. CX model in *B* is after ref. 63, visualized with insectbraindb.org. *C*, *D*, and *E* reprinted from ref. 29, which is licensed under CC BY 4.0.

typically provide input to the CX and distribute activity along a single neuropil or a specific layer, and columnar neurons connect specific columns between different neuropils (27) and finally provide output from the CX.

In the desert locust *Schistocerca gregaria*, intracellular recordings showed that many neurons of the CX are tuned to the polarization angle in the animal's zenith as well as to the azimuth of a simulated sun stimulus (11, 28, 29). In neurons with arborization domains in single columns of the PB, tunings to these cues vary along the 16 columns of the bridge in a topographic manner (28, 29), indicating a compass-like representation of celestial cues, which could be used as a heading estimate suitable to aid spatial navigation. In a similar way, the azimuth of a simulated sun or the orientation of a visual panorama is represented in the PB and CBL of *Drosophila*. However, while recordings across different individuals suggest that the compass representation in the CX of locusts is consistent across animals, in *Drosophila* the representation of azimuthal space shows an individual offset between animals (4, 8, 16).

Owing to the physics of Rayleigh scattering, the position of the sun in the sky is linked to a unique pattern of polarization (Fig. 1*A*). Thus, one might expect that central maps within the CX converge, such that cells within particular columns are excited by the combination of solar azimuth and AoP that would be coupled in a natural sky. Prior research suggests this is not the case, however (29). Whereas the preferred AoP changed across the PB from left to right in a counterclockwise fashion, the preferred azimuth in the same set of neurons changed in a clockwise manner (ref. 29 and Fig. 1 *D* and *E*). It has, therefore, remained unclear how these compass systems may interact to generate a consistent heading estimate.

Studies on homing behavior showed that ants and bees make systematic navigation errors when they were allowed to see just a small part of polarized skylight (30, 31). This is not surprising, given that the full celestial pattern of polarization cannot be unambiguously reconstructed from a narrow aperture and suggests that faithful directional information requires visual input from large parts of the sky. In line with these observations, Bech et al. (32) found that unidentified neurons at the input stage of the locust CX sample polarization information from nearly the entire hemisphere above the animal. The AoP tuning in these neurons varied across the receptive field in a pattern that matched the sky polarization pattern produced by a distinct solar position (32). We show here that several types of neuron in the PB have similar coding properties. Their tunings, moreover, vary topographically depending on the location of their arborizations in the PB and, as a population, cover the full range of azimuthal directions, consistent with a polarization-pattern based sun compass. This compass resembles the azimuth compass that was found in CX neurons when stimulated with an unpolarized light spot simulating the sun (29). The data significantly advance our understanding of the integration of polarization vision in the CX network and support the idea that the locust CX acts as a hub for skylight navigation combining all available cues in the sky to form a robust compass signal.

Results

We recorded intracellularly from AoP-sensitive neurons in the locust CX in order to investigate their tuning properties across the full sky. We stimulated the animals with blue light passed through a rotating polarizer from different positions in the dorsal visual field (Fig. 2*A*). Neurons showed sinusoidal modulation of activity during a 360° rotation of the polarizer (Fig. 2*B*), but the preferred AoP of a single neuron typically varied depending on stimulation position (Fig. 2 *C*–*F*). Tracer injection after measurements allowed for identification of neuron types and reconstruction of their morphology. Recordings from 23 neurons with ramifications in particular columns of the PB of the CX were analyzed. These include four types of columnar neurons with ramifications in single columns of the PB (CL1, 6×; CP2, 1×; CPU1, 4×; and CPU2, 5×) and TB1 tangential neurons (7×) with dendritic and axonal ramifications in particular sets of columns (Fig. 1*C*). The number of stimulation positions ranged from 9 to 33 (median 19; 22 to 33 in CL1, 9 in CP2, 9 to 21 in CPU1, 13 to 18 in CPU2, and 9 to 33 in TB1).

Receptive Fields of CX Neurons Span Large Parts of the Sky. Most previous studies have assessed the AoP sensitivity of CX neurons by stimulation with a rotating polarizer in the animal's zenith. In the present study, we stimulated from positions in the entire dorsal hemisphere of the animal, which allowed us to analyze the AoP sensitivity across the dorsal visual field (Fig. 2). Briefly, we used the R^2 value of the AoP responses as a measure of AoP

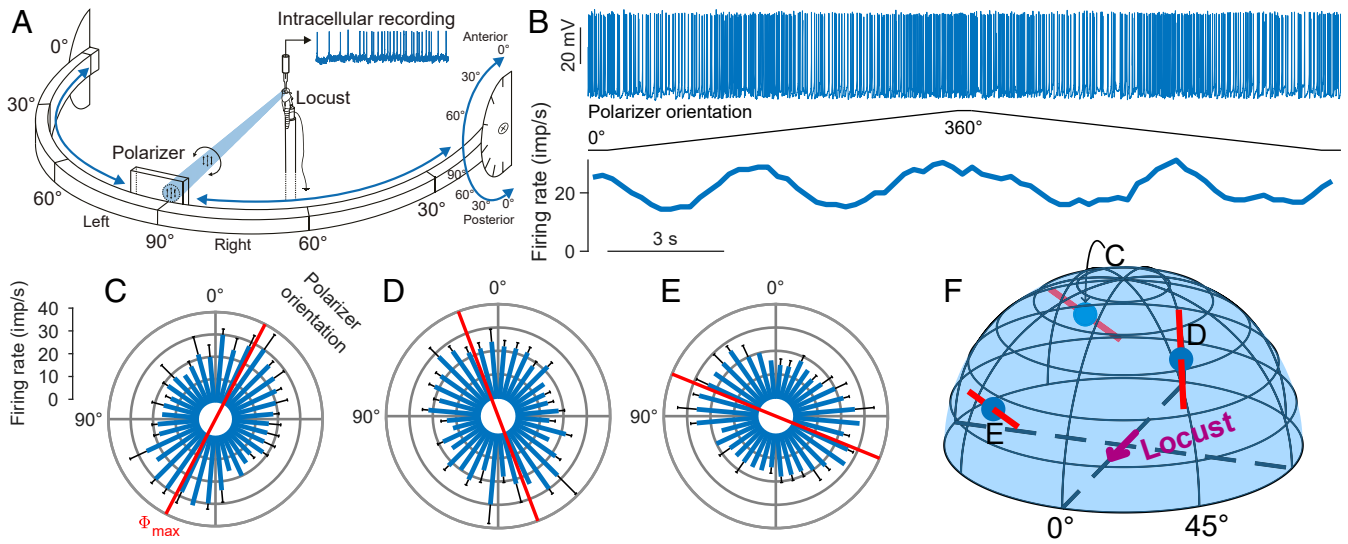

Fig. 2. Polarization sensitivity of a TB1 neuron to stimulation from different points in the virtual sky. (*A*) Experimental setup. Locusts were stimulated with blue light (465 nm) that was passed through a rotating polarizer to assess AoP sensitivity of single cells. The light source was movably mounted on a perimeter that could be tilted, allowing for stimulation from directions in the entire dorsal visual field. Reprinted from ref. 32. Copyright (2014), with permission from Elsevier. (*B*) Spike train (*Top*) of the neuron during rotation of the polarizer at stimulus position C indicated in *F*. Two successive full rotations with opposing turning direction of the polarizer (*Middle*) elicit two activity peaks per rotation (*Bottom*). (*C*) Circular response plot showing the data from *B* after pooling. Responses are pooled by assigning each spike the polarizer orientation at its time of occurrence and treating the resulting angle array as a single set; the preferred AoP (Φ_{max} = 152.4°; red axis) equals the axially corrected average angle of all spikes. The blue bars show the mean binned spike count from both rotations, converted to firing rate; error bars indicate SD. The firing rate is significantly correlated with polarizer orientation (linear-circular correlation, $P < 0.001$, $R^2 = 0.82$). The (azimuth|elevation) stimulus coordinates were (213.7°|25.7°), resulting from the LED positioned at 60° right on the perimeter, the perimeter tilted 30° to posterior. Response plots from the same neuron analogous to *C* at stimulus positions (*D*) (49.1°|48.6°) (LED at 60° left on perimeter, perimeter tilt 60° anterior) and (*E*) (326.3°|25.7°) (LED at 60° right on perimeter, perimeter tilt 30° anterior). Φ_{max} = 20.8° and 67.9°, $P < 0.001$ for all responses, R^2 = 0.49 and 0.79, respectively. (*F*) Illustration of the stimulus positions corresponding to the response data shown in *C*–*E*. Red bars indicate Φ_{max}, and blue dots indicate the spherical stimulus coordinates.

sensitivity, resulting in a sensitivity map for each neuron. We normalized the R^2 values to the value range of each neuron and defined receptive fields as the regions that remained after applying a 75% threshold to these maps (Fig. 3 and *SI Appendix*, Figs. S2 and S3). The fields generally varied in shape and size, in several instances extending from the zenith down to the horizon

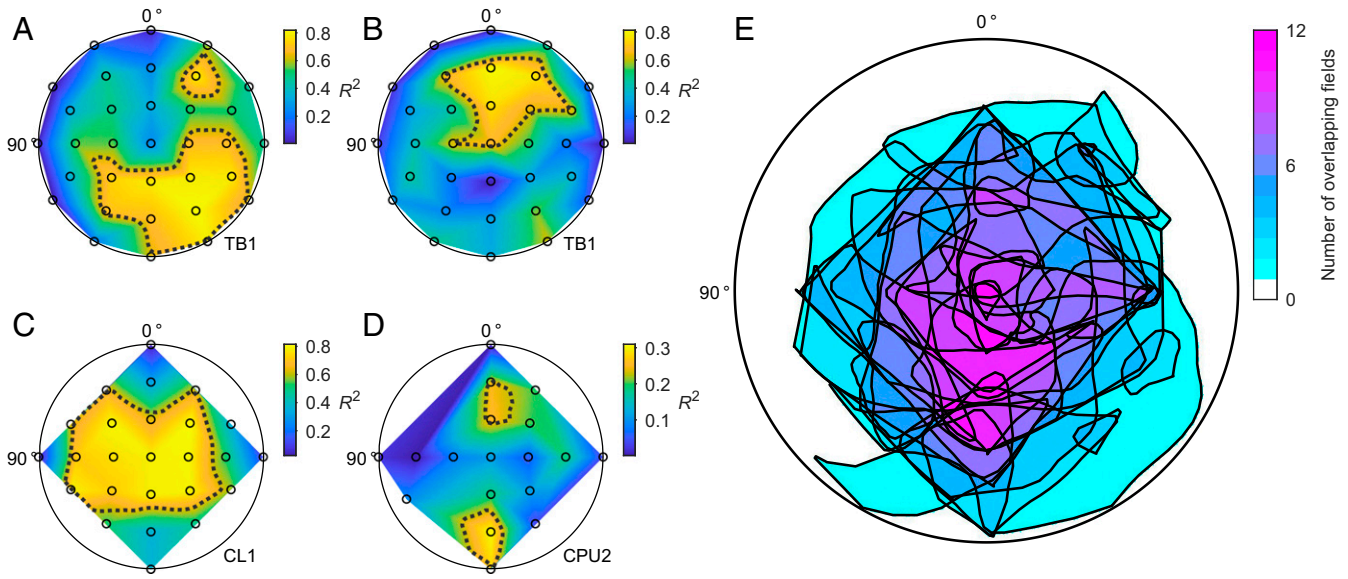

Fig. 3. Receptive fields for AoP sensitivity of CX neurons. (*A*–*D*) Example datasets: polarization sensitivity as a function of stimulus position in the dorsal visual field (view on flattened hemispheres; see *SI Appendix*, Fig. S1, for clarification of the coordinate system) of two TB1 neurons (*A* and *B*), a CL1 neuron (*C*), and a CPU2 neuron (*D*). The sensitivity to polarization angle indicated by the R^2 value of AoP responses is color-coded at each tested position (black circles) and linearly interpolated in between. Dotted lines are smoothed 75% isolines of the normalized R^2 values. (*E*) Superimposed smoothed borders of all 75% fields of all recorded neurons (23 neurons with 31 fields) with color-coded degree of overlap. See *SI Appendix*, Fig. S2, for a graphical description of the analysis; *SI Appendix*, Fig. S3, for the significance of the chosen R^2 threshold; and *SI Appendix*, Fig. S4, for all individual sensitivity maps.

(Fig. 3*A*); some neurons had more than one field (Fig. 3*D*). Based on visual inspection (cf. *SI Appendix*, Fig. S4), we found no trend in field size, shape, or position regarding cell type. Many fields were centered at a medium elevation (Fig. 3 *A*, *B*, and *D*); however, the overlap of all fields was maximum posterior from the zenith at about 60° elevation (Fig. 3*E*).

Neurons in the CX Show Matched-Filter Properties. Extracellular recordings showed previously that neurons of the CBL, most likely TL neurons, possess matched-filter properties (32) for polarization patterns of the blue sky that theoretically allow for unambiguous solar azimuth coding solely based on polarization sensitivity. Using intracellular recordings, we found that other types of CX neuron also show this feature (Fig. 4).

To test whether the measured patterns of preferred AoPs match a particular sky polarization pattern, we fitted them to generated patterns of AoPs that correspond to sky polarization patterns calculated from various solar coordinates (cf. Fig. 1*A*). This procedure yielded a matched-filter tuning in the form of solar coordinates that corresponded to the best matching, or least deviating, sky polarization pattern. Typically, we found a rather conspicuous match between the response pattern and the best matching pattern, with a clear minimum deviation (Fig. 4 *A* and *B*). To statistically assess the fitting quality of the best match, we tested the associated pattern deviation against a bootstrapped population of pattern deviations. This population was calculated from randomized response patterns, generated from the same dataset (Fig. 4*C*); all 6 CL1 neurons, 6 of 7 TB1 neurons, 2 of 4 CPU1 neurons, and 3 of 5 CPU2 neurons (in total 17 of 23 neurons) passed this bootstrap test and were used for further analysis.

Azimuthal Tuning of the Matched Filter Is Represented Topographically along the Protocerebral Bridge. Because preferred zenithal AoPs are topographically represented in the PB (28), we searched for a connection between neuroanatomy and the azimuthal component of the matched-filter tuning. We determined the arborization column in the PB of each neuron based on the tracer injections after recording. Recent work in *Drosophila* strongly suggests that different types of columnar neuron innervating the same column in the PB share a common heading preference (7). Neurobiotin injections showed that our recordings in the locust were from four different types of columnar neuron of the PB and one type of tangential neuron. All neurons arborized in a distinct column (Fig. 1*C*), except for TB1 neurons, for which we considered the ipsilateral column of the PB that is innervated by varicose arborizations. Tuning direction was uniformly distributed in our dataset (Fig. 5*A*) and, when pooling all cell types, was highly correlated with the arborization column in the PB (Fig. 5*B*). The resulting regression indicates that the full range of possible directions around the animal is covered by the solar azimuths of the preferred polarization patterns (Fig. 5*C*).

Discussion

We show here that several types of CX neuron in the locust brain integrate polarization information in the dorsal visual field consistent with a matched filter that is tuned to specific solar polarization patterns. The azimuthal component of this tuning depends on the arborization position in the PB, varying along this neuropil in a topographic manner with full coverage of azimuthal space. This polarization-based sun compass closely resembles the previously reported sun compass derived from unpolarized light stimulation (29), suggesting that these neurons reliably and congruently signal the solar azimuth irrespective of cue modality. Our finding sheds light on polarization vision processing in insects and elucidates its role for the constitution of a sun compass in the insect CX.

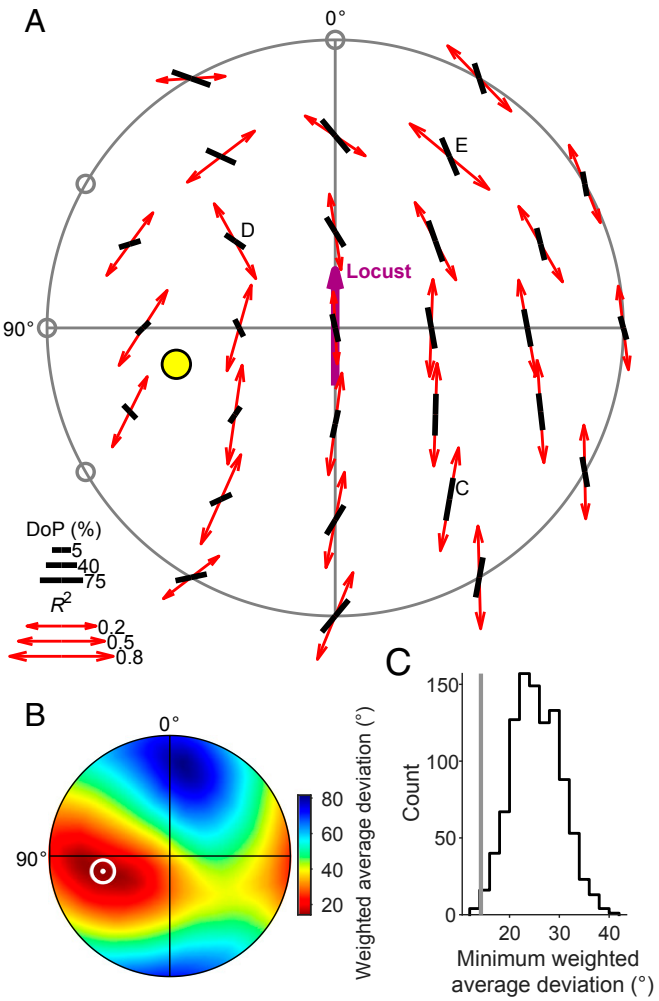

Fig. 4. Receptive fields of CX neurons are matched to sky polarization patterns. (*A*) Top view on the pattern of preferred AoPs (Φ_{max}; red double arrows) of a TB1 neuron and the AoPs that belong to the best-matching sky polarization pattern (black bars). This pattern corresponds to a sun position at 39.1° elevation and 102.9° azimuth (yellow dot). Arrow and bar length scale with response R^2 value and degree of polarization (DoP), respectively; gray circles indicate statistically nonsignificant AoP responses (linear-circular correlation, $P \geq 0.05$). Note that the originally spherical stimulus coordinates and AoP axes were transformed into polar coordinate space for visualization on a flattened hemisphere surface (cf. *SI Appendix*, Fig. S1). The labeled positions refer to the responses of the TB1 neuron shown in Fig. 2; Fig. 3*A* shows the AoP sensitivity map of this dataset. (*B*) Flattened hemispherical heat map of the deviation between the measured Φ_{max} pattern and calculated sky polarization patterns as a function of solar position used for calculation. The pattern deviation for a given solar coordinate is the average of the angular deviations between the Φ_{max} and the sky polarization pattern at each stimulus position, weighted by degree of polarization and R^2 value at each stimulus position. The white dot and circle have the same coordinates as the solar marker in *A* and mark the minimum (14.26°) of the deviations of all tested solar positions (n = 32,760 equally distributed positions). Color scale is shown to the right. (*C*) Distribution of 1,000 bootstrapped pattern deviations of randomized response patterns based on the data in *A* from the resulting best matching polarization pattern. The gray line indicates the observed deviation (14.26°; white marker in *B*), which significantly differs from the bootstrap distribution (P = 0.004, equals the fraction of bootstrapped deviations that are lower than or equal to the observed deviation). See *SI Appendix*, Fig. S7, for all individual response patterns with best-matching sky polarization pattern.

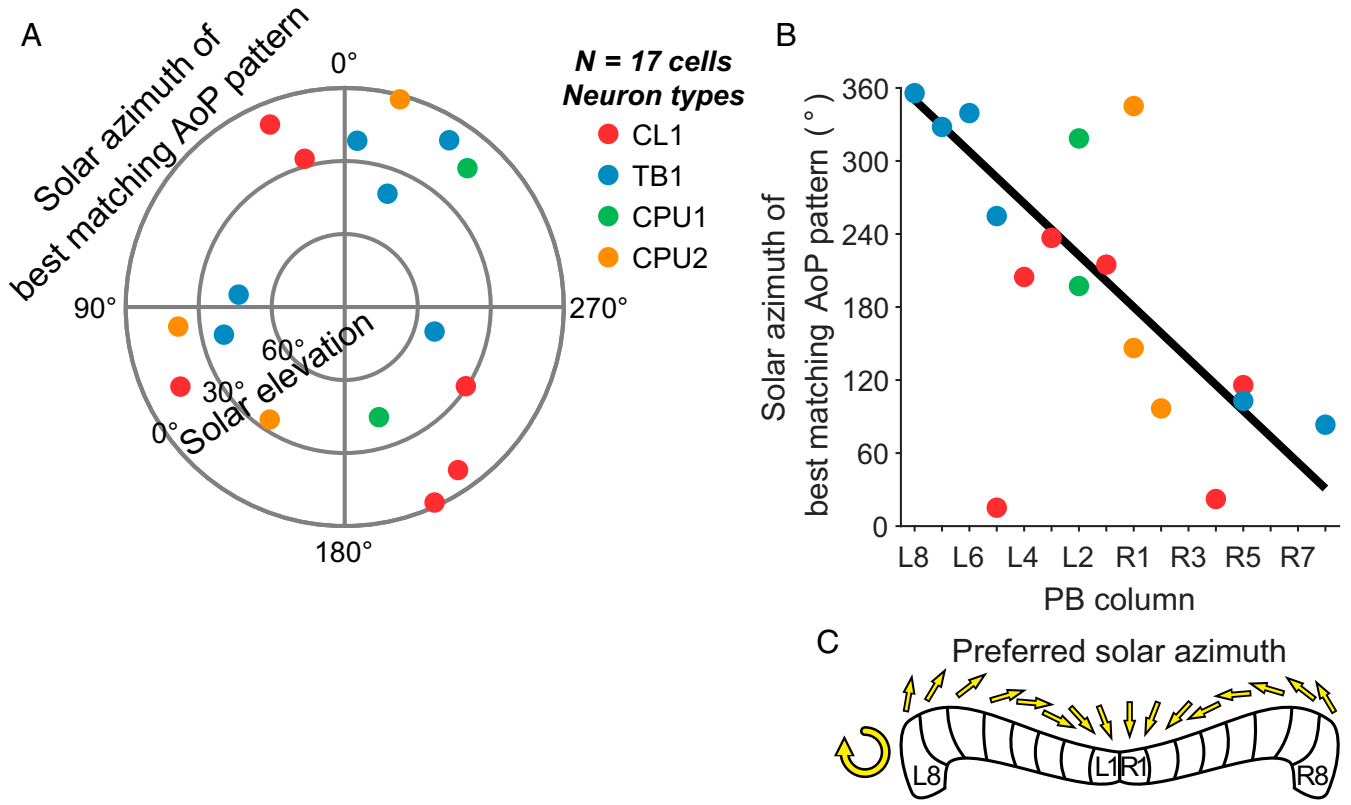

Fig. 5. The azimuthal tuning of matched filters is represented topographically along the PB. (*A*) Polar plot showing the solar positions that correspond to the best matching polarization patterns of single cells. Azimuth data are uniformly distributed (Rayleigh test, $P = 0.89$, $n = 17$). (*B*) Regression diagram of the column of arborization in the PB vs. the azimuthal component of the solar coordinates in *A*. The azimuth depends on PB column (circular–linear correlation, $\rho = -0.51$, $P = 0.028$). The estimated regression covers nearly 360° along the PB ($y = -21.3x + 350.3$; column L8 corresponds to $x = 0$). (*C*) Schematic compass topography according to the resulting regression. The preferred azimuth covers a range of nearly 360° along the PB.

CX Neurons Are AoP Sensitive across the Entire Dorsal Visual Field. Many CX neurons are sensitive to the AoP of light in a large proportion of the locust's dorsal visual field (Fig. 3), which is in line with the receptive field properties of dorsal rim area photoreceptors (33). While the dorsal rim areas are directed toward areas in the sky centered slightly contralaterally from the zenith, they show considerable overlap in the zenith, and the summed receptive fields of their receptors extend far down to the contralateral side, covering most parts of the sky (33). The striking differences in receptive field size and organization of the recorded neurons (Fig. 3 and *SI Appendix*, Fig. S4) were unexpected and suggest major cell-specific differences in input from the right and left dorsal rim ommatidia. Although some receptive fields were substantially offset from the zenith (e.g., Fig. 3*A*), superposition of all fields revealed a mean arrangement symmetric to the midline indicating an overall balanced input from both eyes. The fan-like arrangement of microvilli orientations across the dorsal rim ommatidia in the locust and other insects (34–36) might be a preadaptation to the sky polarization pattern, as suggested by ref. 37, and likely facilitates the matched-filter properties for AoP coding of CX neurons. Inspection of the fitting data shows that at certain points in the sky, the fit between celestial AoP and AoP tuning of the neuron is nearly perfect, while at others, they deviate significantly from each other (Fig. 4*A* and *SI Appendix*, Fig. S5*D*). Mismatches often occurred near the calculated sun position, where the degree of polarization is low (Fig. 4*A* and *SI Appendix*, Fig. S5*D*). These points in the sky would, therefore, contribute only little to the tuning of the neurons. In an area upstream of the CX, the anterior optic tubercle, neurons are even blind to polarization within a circle of 50° around the sun (38). All recordings presented here were obtained from laboratory-raised animals that had not been exposed to a natural sky. This shows that AoP tuning is largely determined genetically but does not exclude that fine tuning of the neurons to sky polarization patterns might require learning-related adaptations when the animals experience a natural sky.

Representation of Heading Directions in the CX. Data from various insect species, specifically fly, dung beetle, butterfly, cockroach, locust and bee, point to a role of the CX in integrating external and self-generated sensory information for the control of goal-directed navigation (27, 39–43). In *Drosophila*, Ca^{2+}-imaging revealed a single bump of activity in the columns of the ellipsoid body (4), the fan-shaped body (7), and the PB (6, 8) of the CX corresponding to a head direction signal based on visual landmark information and self-motion cues (4, 44). Differences in the angular offset between bump position and actual heading in different individual flies together with physiological manipulation of bump position and connectivity data strongly suggest that heading representation is based on a ring attractor network in the ellipsoid body and the PB (9, 45–47). Ring attractor networks have been previously proposed to underlie head direction coding in mammals and are characterized in flies by a single bump of activity within the circular CX network relating directly to an angular direction (3, 9, 48). While in *Drosophila*, emphasis has been on the role of landmark and self-motion cues in driving the position of this bump, sky compass signals, as demonstrated to drive neural activity in CX neurons in the locust, dung beetle, sweat bee, and monarch butterfly (12, 29, 49, 50), apparently play a role in *Drosophila*, too (16). In flies and locusts, directional

heading signals are represented in the CX in a compass-like, topographic fashion (4, 8, 16, 28, 29). In the locust, compass-like representations of zenithal AoP and azimuth of a simulated sun, found in the columns of the PB, are based on recordings from single neurons innervating different columns within the PB (28, 29). Because topographies in the locust were extracted from data obtained from different individual animals, representation of celestial cues appears to be fixed across individuals unlike the highly flexible topography in *Drosophila* (4, 16, 28, 29). Despite these apparent differences in sensory inputs and internal topographies between locust and fly, a ring attractor network as suggested to underlie heading representation in the fly CX may operate in locusts as well (13).

Matched-Filter Tuning Is Topographically Represented in the PB. A puzzling result of the study by Pegel et al. (29) was that the compass representations based on the preference angle of polarized zenithal light (28, 29) and azimuth representation of an unpolarized light spot (29), obtained from the same set of neurons, generated contradicting spatial information (Fig. 1 *D* and *E*) although these cues are tightly coupled under natural conditions and, therefore, should provide the same directional information. Whereas the zenithal AoP preference changed in a counterclockwise manner from PB column L8 to column R8, the preferred azimuth changed in a clockwise fashion. Assessing the matched-filter properties of the neurons for whole-sky polarization tuning allowed us to calculate hypothetical sun positions corresponding to those matched filters. The azimuthal component of these calculated sun positions is again represented topographically along the PB, consistent with a sun compass solely based on the polarization pattern of the sky (Fig. 5 *B* and *C*). This compass covers the full range of directions around the animal, making it suitable to unambiguously signal solar azimuth. The azimuth compass for unpolarized light spots (29), directly indicating the solar position (Fig. 1*E*), is highly similar to the matched-filter polarization compass (Fig. 5 *B* and *C*), both in terms of 360° coverage and sign of the regression slope, i.e., both compasses provide the same output, however, based on different environmental cues.

The compass mismatch reported by Pegel et al. (29) may be based on inadequate compass information provided by the zenithal AoP alone. It has been suggested previously that insects need to perceive large parts of the sky polarization pattern in order to orient correctly: behavioral experiments showed that honey bees make systematic orientation errors when their view on the sky is restricted to a small patch (30, 31). These errors might explain the conflicting outputs of the previously reported azimuth and polarization compasses (29). Because of its 180° periodicity, a single AoP as presented in previous studies does not provide an unambiguous orientation signal, especially if the receptive field center of the recorded neuron is not in the zenith (51), which is the case for several of the neurons studied here. The matched-filter compass, instead, matches well with the azimuth compass because it results from integrating the AoP over large parts of the visual field, which solves the ambiguity that arises from perceiving a single AoP at a small patch in the sky. A recent computational study (52) presenting a model of the insect polarization compass also suggests that the compass output generated under visual stimulation from a single spot conflicts with the output generated under whole-sky stimulation in a similar way as shown by Pegel et al. (29).

The matched-filter polarization compass presented here is based on pooling data from different cell types in the PB and, therefore, assumes that different neurons innervating the same PB column share a common heading preference. This is supported by previous data in locust (28, 29) revealing highly similar tuning preference to zenithal AoP in different types of columnar neuron of the same PB column and by a recent study in *Drosophila*, showing matching bump activity in neurons innervating corresponding columns of the ellipsoid and fan-shaped body (7). In addition, we investigated the impact of each cell type on the regression results and found that the compass topography is robust even when individual cell types are excluded (*SI Appendix*, Fig. S9). Nevertheless, differences between individual animals as well as phase shifts between different cell types might contribute to the relatively high variability of our tuning data (Fig. 5*B*). Because large interindividual differences in the angular offset of activity bump position and environmental cues are a key feature of head direction coding in *Drosophila* (4), a combination of data from different individual flies would most likely not result in a common compass representation across flies.

The CX has been shown to be a navigation hub, and in the desert locust's natural habitat, where local cues are scarce and celestial cues are reliable, it is conceivable that the polarization-based compass proposed in this study pervades the entire network, contributing to robust, multimodal celestial navigation.

Methods

Animals and Preparation. Adult desert locusts (*S. gregaria*), reared under crowded conditions at 28 °C in a 12 h/12 h light/dark cycle, were used for experiments. After removing legs and wings, they were mounted on a metal holder using dental wax. The head capsule was opened frontally, and ocelli and antennae were removed in the process; tracheal, fat, and muscle tissue were partially removed to expose the brain and mechanically isolate it for means of stabilization. The esophagus was cut near the mandibles and removed together with the gut through the abdomen. A twisted metal wire covered in wax, forming a small platform, was placed posterior to the brain and was fixed to the ventral head capsule to increase recording stability. Finally, the neural sheath was partly removed with forceps to allow brain penetration by the recording electrode. Specimens were kept moist during preparation, recording, and dissection with locust saline (53).

Intracellular Recording and Histology. We measured neural activity with sharp microelectrodes drawn from borosilicate capillaries (Hilgenberg) with a Flaming/Brown filament puller (P-97; Sutter Instrument), their tips filled with a solution of Neurobiotin tracer (Vector Laboratories; 4% in 1 M KCl) and shanks filled with 1 M KCl. Signals were amplified ×10 and filtered (Bessel filter, 20-kHz cutoff frequency) with an SEC 05L amplifier (npi electronic GmbH), monitored via a custom-built audio monitor (University of Marburg, Germany) and an oscilloscope (HAMEG Instruments GmbH), digitized with a Power1401-mkII (Cambridge Electronic Design) at 12.5 kHz, recorded with Spike2 (Cambridge Electronic Design), and analyzed offline with custom scripts for MATLAB (MathWorks). After stimulation, Neurobiotin was injected by applying positive current of 0.2 to 2 nA for at least 2 min. For histology, brains were dissected and then fixed overnight in a solution of 4% paraformaldehyde, 0.25% glutaraldehyde, and 0.2% saturated picric acid diluted in 0.1 M PBS and optionally kept at 4 °C in sodium phosphate buffer until further processing. They were rinsed in PBS (4 × 15 min) and incubated with Cy3-conjugated Streptavidin (Dianova; 1:1,000 in PBS with 0.3% Triton X-100 [PBT]) for 3 d at 4 °C. After rinsing in PBT (2 × 30 min) and PBS (3 × 30 min), they were dehydrated in an ascending ethanol series (30%, 50%, 70%, 90%, 95%, and 2 × 100%, 15 min each) and cleared in a 1:1 solution of ethanol (100%) and methyl salicylate for 20 min and in pure methyl salicylate for 35 min, to finally mount them in Permount (Fisher Scientific) between two coverslips. To identify cell morphologies, specimens were scanned with a confocal laser-scanning microscope (Leica TCS SP5; Leica Microsystems). Cy3 fluorescence was elicited with a diode-pumped solid-state laser at 561 nm wavelength. Image stacks were then processed into maximum intensity projections using Fiji (54, 55), and projections were edited in Adobe Photoshop and Illustrator (Adobe Systems Inc.). Ramification domains of neurons were deduced from their relative position within neuropils, identifiable through tissue autofluorescence, and morphological characteristics as described previously (56, 57).

Stimulation. Animals were stimulated with polarized blue light (465 nm) from various directions as previously described (32), except that we added a diffuser between LED (ELJ-465-627; Roithner LaserTechnik) and polarizer (HN38S; Polaroid), which resulted in a photon flux of 7.76×10^{13} photons $\cdot$ cm^{-2} $\cdot$ s^{-1}. Briefly, we measured the preferred AoP of single cells depending on stimulus position in the animal's dorsal visual field, ranging

down to 0° elevation. We successively stimulated from 33 positions, each stimulation composed of three consecutive full rotations of the polarizer at 40° · s^{-1}: a counterclockwise rotation of the polarizer, which was discarded to exclude artifacts from phasic light-on responses, and one clockwise and another counterclockwise rotation, which were averaged to calculate the preferred AoP. Testing all stimulus positions took roughly 40 min; in some cases, not all 33 positions could be tested due to instability of recordings.

Data Evaluation.

Calculating preferred AoP. Action potentials were assigned the orientation of the polarizer at the respective timing; the resulting angles were multiplied by 2 for axial correction, averaged using the *CircStat* toolbox (58), and divided by 2, yielding the preferred AoP during this rotation. Averaging multiple rotations was done by pooling all angles and then averaging them as above. To statistically assess a response, we binned the data in 10° bins and tested the resulting bin counts for correlation with bin angles using linear-circular correlation analysis (58), yielding a P value, correlation coefficient, and coefficient of determination (R^2). Neuronal activity was considered to be significantly modulated by the presented AoP if P was < 0.05. Circular histograms were created with the *CircHist* package (59).

Calculating the best-matching polarization pattern. The same procedure was applied as previously described (32), with minor differences, and is summarized conceptually here (see *SI Appendix, Methods* and Figs. S5 and S6, for extended information). Briefly, we compared the pattern of preferred AoPs in the dorsal hemisphere with polarization patterns that would arise from specific solar positions to obtain one best-matching pattern. The azimuthal component of the solar position that belonged to this pattern was considered to be the preferred solar azimuth of the recorded cell. Solar polarization patterns were generated from 32,760 (360 × 91) virtually equally spaced solar positions on a dense hemispherical Fibonacci grid (60) with a spacing of 0.022° ± (8.7×10^{-5})° (average angle ±95% confidence interval) distance to the nearest neighbor. For each solar position, the AoP and degree of polarization were calculated at those positions that the animal was stimulated from, based on the single-scattering Rayleigh model (61) (Fig. 1*A*). At each stimulus position, the unsigned angular difference between the measured preferred AoP and the pattern's AoP at this position was calculated. Only AoP responses with statistically significant modulation were used. Angular differences were averaged, each difference weighted by the degree of polarization, the response-correlation's R^2 value, and the normalized sum of the arc distances to the nearest 22% of stimulus positions. This yielded a solar position-specific average deviation between the polarization pattern as generated from the sun at this position and the neuron's pattern of preferred AoPs. The polarization pattern corresponding to the solar position with the lowest deviation was considered the best-matching pattern, meaning that the perception of a full polarization pattern as produced by the sun at this position should evoke the highest neuronal activity in the recorded neuron. The dependence of the azimuth of this preferred solar position on the column of neural arborization was tested using circular–linear correlation analysis (62).

Bootstrapping. To classify the magnitude of pattern deviations—whether the lowest pattern deviation is objectively low—we implemented a bootstrapping procedure that created a population of 1,000 randomized samples for each dataset. A randomized sample was obtained by randomly drawing (with replacement) stimulus responses from the pool of measured responses that showed a statistically significant activity modulation and distributing them on all stimulus positions used during this experiment. Each sample was treated as described above for real datasets, yielding a best-matching polarization pattern and its average deviation from the randomized response pattern. We then used the population of randomization-based pattern deviations to classify the minimum pattern deviation of the actual dataset by calculating a bootstrap P value with $P(D) = \frac{\sum_{k=1}^{b} [d_k \leq D]}{b}$, where D is the minimum pattern deviation of the actual dataset, k is the bootstrap sample index, b is the number of samples (1,000), and d_k is the minimum pattern deviation of the kth sample. Simply put, P equals the fraction of the number of bootstrapped minimum pattern deviations that are less than or equal to the minimum pattern deviation of the actual dataset. We considered D to be objectively low if $P(D) < 0.05$, which is equivalent to D being below the 5% percentile of the bootstrap population. From a total of 23 datasets, this was the case for 17; only these were used for further analysis of matched-filter tuning (cf. *SI Appendix*, Fig. S8, for the same analysis based on all datasets).

Estimating visual fields. We calculated the dimensions of visual fields based on the R^2 value of AoP responses. Briefly, we excluded data points for which the response's normalized (per neuron) R^2 value was below 0.75 and assigned the remaining data points to clusters based on their distance to one another (see *SI Appendix*, Fig. S2, for a detailed graphical description). First, we created a hemispherical Fibonacci grid (60) of 2,500 virtually equally distributed points. To simplify calculations, we flattened the grid and the spherical data points that referred to the stimulation positions by converting them to polar coordinates where the center (radius $\rho = 1$) corresponds to the zenith and points with $\rho = 1$ and arbitrary θ correspond to the spherical coordinate with 0° elevation and θ azimuth. To facilitate the next steps, these coordinates were further converted to planar Cartesian coordinates. We then linearly interpolated the R^2 values at the stimulation positions over the generated grid using MATLAB's *scatteredInterpolant* function. Points that were outside the convex hull built from the Delaunay-triangulated stimulation positions were discarded; this way, only the part of the visual field being enclosed by the outermost (relative to the zenith as center) stimulus positions was considered. The interpolated R^2 values were normalized to their range, and all data points where $R^2_{norm} < 0.75$ were discarded. This resulted in one or more clouds of data points on the flattened visual field of the animal where the AoP response was relatively high; we considered these clouds the receptive fields of the recorded cell. We then used a hierarchical cluster analysis approach in order to objectively separate the resulting clouds from one another and categorize them into individual receptive fields. First, the points were converted back to spherical coordinates, and their pairwise distances were calculated with the *pdist* function using the great-circle distance as the distance measure. Cluster trees were generated with the *linkage* function; to find the linkage method that resulted in a tree that described the distance relationships in the data best, we used *cophenet* to calculate the cophenetic correlation coefficient for each method and used the one with the highest coefficient. We then used *evalclusters* with the gap criterion, also called "elbow method," and the silhouette criterion to find the optimal number of clusters in the tree; separation into maximal six clusters was considered. The optimal number of clusters was chosen based on visual inspection of the raw clusters and the cluster tree and on the tree evaluation.

Data Availability. Physiological recordings, neural morphologies, and MATLAB code have been deposited in data_UMR for public access (https://dx.doi.org/10.17192/fdr/22 and https://dx.doi.org/10.17192/fdr/23) (64, 65).

ACKNOWLEDGMENTS. We thank Dr. Stephanie Wegener and Jann Goschenhofer for initial discussions on the bootstrap procedure, Dr. Naomi Takahashi for supplying additional data, Dr. Basil el Jundi for helpful discussions on the manuscript draft, and Martina Kern for maintaining locust cultures. This work was funded by DFG (Deutsche Forschungsgemeinschaft, German Research Foundation) grants HO 950/24-1 and HO 950/25-1 to U.H.

1. J. S. Taube, Head direction cells and the neurophysiological basis for a sense of direction. *Prog. Neurobiol.* **55**, 225–256 (1998).
2. J. S. Taube, The head direction signal: Origins and sensory-motor integration. *Annu. Rev. Neurosci.* **30**, 181–207 (2007).
3. D. E. Angelaki, J. Laurens, The head direction cell network: Attractor dynamics, integration within the navigation system, and three-dimensional properties. *Curr. Opin. Neurobiol.* **60**, 136–144 (2020).
4. J. D. Seelig, V. Jayaraman, Neural dynamics for landmark orientation and angular path integration. *Nature* **521**, 186–191 (2015).
5. A. G. Varga, R. E. Ritzmann, Cellular basis of head direction and contextual cues in the insect brain. *Curr. Biol.* **26**, 1816–1828 (2016).
6. J. Green, V. Vijayan, P. Mussells Pires, A. Adachi, G. Maimon, A neural heading estimate is compared with an internal goal to guide oriented navigation. *Nat. Neurosci.* **22**, 1460–1468 (2019).
7. H. M. Shiozaki, K. Ohta, H. Kazama, A multi-regional network encoding heading and steering maneuvers in *Drosophila*. *Neuron* **106**, 126–141.e5 (2020).
8. J. Green *et al.*, A neural circuit architecture for angular integration in *Drosophila*. *Nature* **546**, 101–106 (2017).
9. S. S. Kim, H. Rouault, S. Druckmann, V. Jayaraman, Ring attractor dynamics in the *Drosophila* central brain. *Science* **356**, 849–853 (2017).
10. S. S. Kim, A. M. Hermundstad, S. Romani, L. F. Abbott, V. Jayaraman, Generation of stable heading representations in diverse visual scenes. *Nature* **576**, 126–131 (2019).
11. U. Pegel, K. Pfeiffer, U. Homberg, Integration of celestial compass cues in the central complex of the locust brain. *J. Exp. Biol.* **221**, jeb171207 (2018).
12. S. Heinze, S. M. Reppert, Sun compass integration of skylight cues in migratory monarch butterflies. *Neuron* **69**, 345–358 (2011).
13. T. Stone *et al.*, An anatomically constrained model for path integration in the bee brain. *Curr. Biol.* **27**, 3069–3085.e11 (2017).
14. B. el Jundi *et al.*, Neural coding underlying the cue preference for celestial orientation. *Proc. Natl. Acad. Sci. U.S.A.* **112**, 11395–11400 (2015).
15. P. T. Weir, M. H. Dickinson, Flying *Drosophila* orient to sky polarization. *Curr. Biol.* **22**, 21–27 (2012).

16. Y. M. Giraldo *et al*., Sun navigation requires compass neurons in *Drosophila*. *Curr. Biol.* **28**, 2845–2852.e4 (2018).
17. K. Fent, Polarized skylight orientation in the desert ant *Cataglyphis*. *J. Comp. Physiol. A Neuroethol. Sens. Neural Behav. Physiol.* **158**, 145–150 (1986).
18. M. L. Brines, J. L. Gould, Bees have rules. *Science* **206**, 571–573 (1979).
19. S. M. Reppert, H. Zhu, R. H. White, Polarized light helps monarch butterflies navigate. *Curr. Biol.* **14**, 155–158 (2004).
20. B. el Jundi, J. Smolka, E. Baird, M. J. Byrne, M. Dacke, Diurnal dung beetles use the intensity gradient and the polarization pattern of the sky for orientation. *J. Exp. Biol.* **217**, 2422–2429 (2014).
21. D. Brunner, T. Labhart, Behavioural evidence for polarization vision in crickets. *Physiol. Entomol.* **12**, 1–10 (1987).
22. M. Mappes, U. Homberg, Behavioral analysis of polarization vision in tethered flying locusts. *J. Comp. Physiol. A Neuroethol. Sens. Neural Behav. Physiol.* **190**, 61–68 (2004).
23. T. L. Warren, P. T. Weir, M. H. Dickinson, Flying *Drosophila melanogaster* maintain arbitrary but stable headings relative to the angle of polarized light. *J. Exp. Biol.* **221**, jeb177550 (2018).
24. T. F. Mathejczyk, M. F. Wernet, Heading choices of flying *Drosophila* under changing angles of polarized light. *Sci. Rep.* **9**, 16773 (2019).
25. T. Labhart, E. P. Meyer, Detectors for polarized skylight in insects: A survey of ommatidial specializations in the dorsal rim area of the compound eye. *Microsc. Res. Tech.* **47**, 368–379 (1999).
26. U. Homberg, S. Heinze, K. Pfeiffer, M. Kinoshita, B. el Jundi, Central neural coding of sky polarization in insects. *Philos. Trans. R. Soc. Lond. B Biol. Sci.* **366**, 680–687 (2011).
27. K. Pfeiffer, U. Homberg, Organization and functional roles of the central complex in the insect brain. *Annu. Rev. Entomol.* **59**, 165–184 (2014).
28. S. Heinze, U. Homberg, Maplike representation of celestial *E*-vector orientations in the brain of an insect. *Science* **315**, 995–997 (2007).
29. U. Pegel, K. Pfeiffer, F. Zittrell, C. Scholtyssek, U. Homberg, Two compasses in the central complex of the locust brain. *J. Neurosci.* **39**, 3070–3080 (2019).
30. S. Rossel, R. Wehner, The bee's map of the e-vector pattern in the sky. *Proc. Natl. Acad. Sci. U.S.A.* **79**, 4451–4455 (1982).
31. S. Rossel, R. Wehner, How bees analyse the polarization patterns in the sky. *J. Comp. Physiol. A Neuroethol. Sens. Neural Behav. Physiol.* **154**, 607–615 (1984).
32. M. Bech, U. Homberg, K. Pfeiffer, Receptive fields of locust brain neurons are matched to polarization patterns of the sky. *Curr. Biol.* **24**, 2124–2129 (2014).
33. F. Schmeling, J. Tegtmeier, M. Kinoshita, U. Homberg, Photoreceptor projections and receptive fields in the dorsal rim area and main retina of the locust eye. *J. Comp. Physiol. A Neuroethol. Sens. Neural Behav. Physiol.* **201**, 427–440 (2015).
34. U. Homberg, A. Paech, Ultrastructure and orientation of ommatidia in the dorsal rim area of the locust compound eye. *Arthropod Struct. Dev.* **30**, 271–280 (2002).
35. S. Heinze, "Polarized-light processing in insect brains: Recent insights from the desert locust, the monarch butterfly, the cricket, and the fruit fly" in *Polarized Light and Polarization Vision in Animal Sciences*, G. Horváth, Ed. (Springer, 2014), pp. 61–111.
36. P. T. Weir *et al*., Anatomical reconstruction and functional imaging reveal an ordered array of skylight polarization detectors in *Drosophila*. *J. Neurosci.* **36**, 5397–5404 (2016).
37. S. Rossel, R. Wehner, Polarization vision in bees. *Nature* **323**, 128–131 (1986).
38. K. Pfeiffer, M. Negrello, U. Homberg, Conditional perception under stimulus ambiguity: Polarization- and azimuth-sensitive neurons in the locust brain are inhibited by low degrees of polarization. *J. Neurophysiol.* **105**, 28–35 (2011).
39. S. Heinze, Unraveling the neural basis of insect navigation. *Curr. Opin. Insect Sci.* **24**, 58–67 (2017).
40. B. el Jundi, E. Baird, M. J. Byrne, M. Dacke, The brain behind straight-line orientation in dung beetles. *J. Exp. Biol.* **222**, jeb192450 (2019).
41. A. G. Varga, N. D. Kathman, J. P. Martin, P. Guo, R. E. Ritzmann, Spatial navigation and the central complex: Sensory acquisition orientation and motor control. *Front. Behav. Neurosci.* **11**, 4 (2017).
42. D. B. Turner-Evans, V. Jayaraman, The insect central complex. *Curr. Biol.* **26**, R453–R457 (2016).
43. A. Honkanen, A. Adden, J. da Silva Freitas, S. Heinze, The insect central complex and the neural basis of navigational strategies. *J. Exp. Biol.* **222**, jeb188854 (2019).
44. D. Turner-Evans *et al*., Angular velocity integration in a fly heading circuit. *eLife* **6**, e23496 (2017).
45. K. S. Kakaria, B. L. de Bivort, Ring attractor dynamics emerge from a spiking model of the entire protocerebral bridge. *Front. Behav. Neurosci.* **11**, 8 (2017).
46. R. Franconville, C. Beron, V. Jayaraman, Building a functional connectome of the *Drosophila* central complex. *eLife* **7**, e37017 (2018).
47. J. Green, G. Maimon, Building a heading signal from anatomically defined neuron types in the *Drosophila* central complex. *Curr. Opin. Neurobiol.* **52**, 156–164 (2018).
48. J. J. Knierim, K. Zhang, Attractor dynamics of spatially correlated neural activity in the limbic system. *Annu. Rev. Neurosci.* **35**, 267–285 (2012).
49. B. el Jundi, K. Pfeiffer, S. Heinze, U. Homberg, Integration of polarization and chromatic cues in the insect sky compass. *J. Comp. Physiol. A Neuroethol. Sens. Neural Behav. Physiol.* **200**, 575–589 (2014).
50. B. el Jundi, J. J. Foster, M. J. Byrne, E. Baird, M. Dacke, Spectral information as an orientation cue in dung beetles. *Biol. Lett.* **11**, 20150656 (2015).
51. K. Pfeiffer, U. Homberg, Coding of azimuthal directions via time-compensated combination of celestial compass cues. *Curr. Biol.* **17**, 960–965 (2007).
52. E. Gkanias, B. Risse, M. Mangan, B. Webb, From skylight input to behavioural output: A computational model of the insect polarised light compass. *PLOS Comput. Biol.* **15**, e1007123 (2019).
53. A. N. Clements, T. E. May, Studies on locust neuromuscular physiology in relation to glutamic acid. *J. Exp. Biol.* **60**, 673–705 (1974).
54. J. Schindelin *et al*., Fiji: An open-source platform for biological-image analysis. *Nat. Methods* **9**, 676–682 (2012).
55. C. A. Schneider, W. S. Rasband, K. W. Eliceiri, NIH image to ImageJ: 25 years of image analysis. *Nat. Methods* **9**, 671–675 (2012).
56. S. Heinze, U. Homberg, Neuroarchitecture of the central complex of the desert locust: Intrinsic and columnar neurons. *J. Comp. Neurol.* **511**, 454–478 (2008).
57. M. J. Beetz, B. el Jundi, S. Heinze, U. Homberg, Topographic organization and possible function of the posterior optic tubercles in the brain of the desert locust *Schistocerca gregaria*. *J. Comp. Neurol.* **523**, 1589–1607 (2015).
58. P. Berens, CircStat: A MATLAB toolbox for circular statistics. *J. Stat. Soft.* **31**, 1–21 (2009).
59. F. Zittrell, CircHist: Circular histogram in MATLAB. https://dx.doi.org/10.5281/zenodo.3445083. Accessed 19 March 2020.
60. R. Swinbank, R. J. Purser, Fibonacci grids: A novel approach to global modelling. *Q. J. R. Meteorol. Soc.* **132**, 1769–1793 (2006).
61. J. W. Strutt, XV. On the light from the sky, its polarization and colour. *Phil. Mag.* **41**, 107–120–274–279 (1871).
62. R. Kempter, C. Leibold, G. Buzsáki, K. Diba, R. Schmidt, Quantifying circular-linear associations: Hippocampal phase precession. *J. Neurosci. Methods* **207**, 113–124 (2012).
63. A. E. Kurylas, T. Rohlfing, S. Krofczik, A. Jenett, U. Homberg, Standardized atlas of the brain of the desert locust, *Schistocerca gregaria*. *Cell Tissue Res.* **333**, 125–145 (2008).
64. F. Zittrell, MATLAB code files from "Matched-filter coding of sky polarization results in an internal sun compass in the brain of the desert locust." data_UMR. Available at https://dx.doi.org/10.17192/fdr/22. Deposited 26 June 2020.
65. F. Zittrell, Raw data: Recording files and microscope image stacks from "Matched-filter coding of sky polarization results in an internal sun compass in the brain of the desert locust." data_UMR. Available at https://dx.doi.org/10.17192/fdr/23. Deposited 26 June 2020.